Wideband Spectrum Sensing and Non-Parametric Signal Classification for Autonomous Self-Learning Cognitive Radios

Mario Bkassiny, *Student Member, IEEE*, Sudharman K. Jayaweera, *Senior Member, IEEE*, Yang Li, and Keith A. Avery

***Abstract*—This paper presents an autonomous cognitive radio (CR) architecture, referred to as the *Radiobot*. This model goes beyond adaptive radio systems to exploit the main ingredients of cognition which, in this context, are mainly self-learning and self-reconfiguration. Without any prior knowledge of the RF environment, the Radiobot applies a sequence of increasingly sophisticated processing steps to detect and identify the sensed signals. In particular, in this paper, it applies a blind energy detection followed by a cyclostationary detection method to detect the active signals and extract their underlying periodic properties as reflected in cyclic frequencies. These extracted signal features are classified based on the Chinese restaurant process (CRP) and a learning algorithm is applied to achieve autonomous self-reconfiguration of the sensing module. We analyze the impact of fading and Doppler frequency shift on both the energy and cyclostationary detections, and show the receiver operating characteristic (ROC) of the carrier frequency detector. We show the robustness of the cyclostationary detection against channel fading and wide-sense stationary noise. Simulation results are presented to verify the multi-band operability and the reconfiguration ability of the Radiobot and to verify the convergence of the proposed learning algorithm.**

***Index Terms*—Cognitive radios, Radiobot, cyclostationary detection, Chinese restaurant process, Dirichlet process, threshold-learning.**

I. Introduction

In literature that followed the original concept of cognitive radios (CR's) given in [1], the CR's have mainly been aimed at achieving dynamic spectrum sharing (DSS) and increasing the spectrum utilization [2]–[4]. However, as highlighted in [5], [6], CR's can have much broader and more ambitious goals. Towards this end, the authors in [5] defined a futuristic CR architecture that emphasizes main features of cognition, namely, (a) the ability for autonomous decision-making/reasoning and learning, and (b) the ability to modify radios behavior based on self-learning. To avoid confusion with previous CR's, the proposed architecture was referred to as the *Radiobot* [5] and it attempts to combine the state-of-the-art models of CR with the notion of autonomous robots.

Manuscript received August 9, 2011; revised February 1 and April 18, 2012; accepted April 22, 2012. The associate editor coordinating the review of this paper and approving it for publication was Y. J. Zhang.

M. Bkassiny, S. K. Jayaweera, and Y. Li are with the Department of Electrical and Computer Engineering, University of New Mexico, Albuquerque, NM, USA (e-mail: {bkassiny, jayaweera, yangli}@ece.unm.edu).

K. A. Avery is with the Space Vehicles Directorate, Air Force Research Laboratory (AFRL), Kirtland AFB, Albuquerque, NM, USA.

Digital Object Identifier 10.1109/TWC.2012.051512.111504

The Radiobots, as presented in [5], are not simply adaptive radios, such as the architectures in [7], [8]. Indeed, they are capable of *self-managing and self-reconfiguring in real-time to match their RF environment while continuously self-learning from their past experience.* In contrast with previous CR architectures that are aiming at improving the spectrum utilization [3], [4], [8], [9], the Radiobots are expected to have all of the following capabilities: 1) autonomous operation, 2) spectrum coexistence/efficiency including dynamic spectrum sharing (DSS), 3) inter-operability in heterogeneous RF network environments, 4) simultaneous operation over multiple modes/networks, and 5) power efficient green communications [5].

The Radiobot can be modeled as a *rational* radio agent that interacts with its RF environment to achieve its communications objectives. A cognitive engine (CE) constitutes the *brain* of the Radiobot [5] and coordinates its decision-making activities. For example, the CE determines the sensing policy, the sensing antenna configurations, etc, for spectrum awareness and also be responsible for making the channel and power allocations for actual communication based on certain system requirements. A high-level system architecture of a Radiobot is shown in Fig. 1 which highlights the two main functions of the CE: 1) Controlling the sensing module and 2) controlling the PHY/MAC communication modules. In order to realize a complete Radiobot system, both autonomous sensing and PHY/MAC decision-making need to be developed. In this paper, however, we restrict our attention to the spectrum sensing module and develop blind autonomous sensing algorithms that can be adapted, through cognitive learning, to unknown RF environments.

According to [5], one of the most important abilities of a Radiobot is to be aware of the RF environment in order to self-characterize the best possible communications mode. To achieve this, it is not sufficient for a Radiobot to just detect the existence of RF activities in its environment, but also it has to be able to identify the *types* of active signals. For example, if the Radiobot identifies a jamming signal at a certain frequency band, it might need to avoid this band so that it preserves the security and reliability of its communication.

In order to detect and identify RF activities, in this paper, we develop a growingly sophisticated signal processing sequence based on blind joint energy/cyclostationary detection. In the first step, energy detection is applied to detect the active

carrier frequencies in the frequency range of interest. Next, a cyclostationarity-based feature extraction algorithm is used to detect the cyclic frequency components at each detected carrier frequency. In contrast with similar two-stage spectrum sensing architectures that assume prior knowledge of the primary channels [10], [11], our proposed spectrum sensing does not require any *a priori* knowledge of the existing channels, which makes it a suitable platform for autonomous Radiobots that operate in unknown RF environments. The performance of the carrier frequency detector is evaluated through its Receiver Operating Characteristic (ROC) and the cyclostationary detection is evaluated for a wide range of SNR and for different sensing times.

Several signal classification and feature extraction methods for CR spectrum sensing have been proposed in the literature, including the models in [12], [13] which rely on support vector machines (SVM's). In this paper, however, we employ non-parametric learning for autonomous signal identification/classification. Thus, our Radiobot extracts a feature vector from each combined energy/cyclostationary detection outcome itself. A feature classification technique, based on the Chinese Restaurant Process (CRP), then permits classifying the obtained features into clusters corresponding to different wireless systems. This proposed non-parametric classification algorithm employs the Dirichlet Process (DP) [14] priors to learn the distribution of clusters within the feature space. The CRP-based classification method was also used in [15], which, however, was only limited to the energy detection.

After each action and/or observation, the Radiobot also applies a learning algorithm to improve its future sensing and communications techniques based on its past experience, as encapsulated in the Observe-Decide-Act-Learn (ODAL) cognition cycle of [5]. Several learning algorithms have been previously applied to CR's for PHY/MAC decision-making. In particular, the reinforcement learning (RL) has been applied for power control [16] and for distributed Medium Access Control (MAC) in CR networks [17], [18]. In our case, however, the Radiobot employs a learning algorithm similar to [19], allowing online self-reconfiguration of the spectrum sensing module. The learning algorithm controls the threshold value of the cyclostationary detector to achieve a certain false alarm probability. In [19], the algorithm estimates the false alarm probability during a training period in which the signals are drawn from a null-hypothesis (denoting no signals). In our case, however, by using the energy detection results, the false alarm probability of the cyclostationary detector can be updated during the normal operation of the Radiobot when no signals are detected.

The remainder of this paper is organized as follows: In Section II, we introduce the Radiobot system sensing model, the RF activity feature extraction techniques, and analyze the impact of superposed multiple RF signals on the feature extraction operation. In Sections III and IV, we analyze the impact of wireless channel fading on both the cyclostationary and carrier frequency detectors, respectively. The CRP-based signal classification algorithm is discussed in Section V. In Section VI, we present the self-reconfiguration of the sensing module. We show the simulation results in Section VII and conclude the paper in Section VIII.

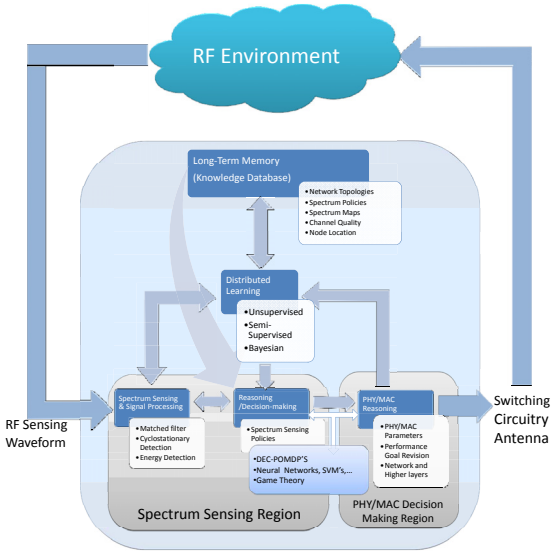

Fig. 1. The actions of the cognitive engine: Sensing and PHY/MAC reconfigurations.

II. System Model

The ability to sense the surrounding RF spectrum is crucial to everything a Radiobot can perform and achieve, due to the fact that spectrum sensing measurements are to be used in (a) detecting, identifying and classifying the signals present in the Radiobots RF environment, and (b) making decisions on its operating mode and subsequent sensing. In practice, a critical limitation of spectrum sensing systems stems from the sampling hardware and the analog-to-digital converters (ADC's) [20]. The tradeoff is between the sampling rate and the resolution. For example, recent research has led to an ADC that can sample at a rate of $16GS/s$ but only with a 6-bit resolution [21]. Better resolutions can only be obtained at the expense of lower sampling rates, as in the case of the 1GS/s ADC *ADS5400* [22] which allows 12-bit resolution. In order to avoid aliasing, the sampling rate is required to be at least as large as the Nyquist frequency. In our case, since the total bandwidth of the spectrum of interest is generally in the scale of several Giga Hertz, it may not be realistic at the current state of the art to expect an ADC to sample, for example, the whole UWB spectrum at a sufficiently high sampling rate with sufficient resolution. A solution is to segment the spectrum of interest into several sub-bands and down-convert each sub-band to intermediate frequency (IF) for sampling. Another solution for wide-band spectrum sensing based on sub-Nyquist sampling was proposed in [23]. However, this technique can only be applied when the signals are sparse.

Similar to other mobile communication systems, hardware compactness is also a major concern. This makes it desirable to reduce the number of hardware components and to avoid parallel RF hardware redundancies. For instance, a communication system may have to be restricted to a limited number of RF mixers used for IF conversions. To address such hardware limitations, we propose a round-robin style joint energy/cyclostationarity-based spectrum sensing strategy. We assume that the RF environment of interest is firstly segmented

$$y(t) = \Re\left\{\sum_{l=1}^{N(t)}\left[\left(\int_0^{\infty} x_l(t-\tau')h_l(\tau',t)d\tau'\right)e^{j2\pi\left(f_{c_l}-f_I\right)t}\right]\right\} + w(t), \quad (1)$$

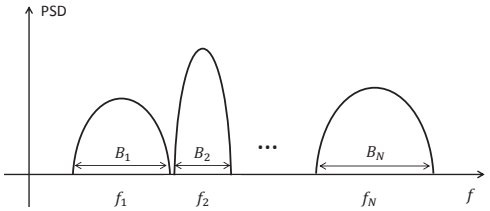

Fig. 2. The wide spectrum of interest is divided into N disjoint wide sub-bands for the purpose of sequential processing.

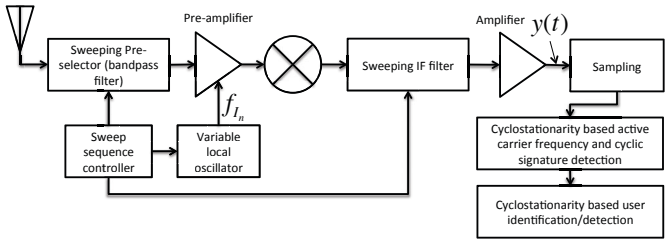

Fig. 3. The cyclostationarity based RF signal detection with a scanning superheterodyne receiver.

into a number of N disjoint, still wide, sub-bands, as shown in Fig. 2.

We assume that these sub-bands are arbitrarily centered at frequencies $f_1, \cdots, f_N$, with bandwidths of $B_1, \cdots, B_N$. It is expected that this segmentation of the spectrum of interest into sub-bands will essentially be determined by the sensing antenna system in use. For example, the reconfigurable sensing antenna system that was developed in [24] in a parallel research effort, is capable of scanning the UWB spectrum by segmenting it into $N = 5$ sub-bands. In particular, this wideband sensing antenna was shown to be able to scan the spectrum from $2 - 10$GHz in $N = 5$ bands, with $f_1 = 2.55$GHz, $f_2 = 3.2$GHz, $f_3 = 4.48$GHz, $f_4 = 5.8$GHz, and $f_5 = 8.15$GHz [24].

We assume that the Radiobot system sequentially picks one of the N sub-bands to sample at each time instant. In order to reduce the requirements on the sampling rate, as shown in Fig. 3, a local variable oscillator with frequency f_{I_n} and a corresponding digital bandpass filter is used to convert the received signal into an IF signal, where we denote by f_{I_n} the local oscillator frequency tuned for the n-th sub-band. By sequentially sensing the N sub-bands, the Radiobot can scan the whole spectrum without requiring parallel hardware nor unrealistic ADC's. Note that, sequential spectrum sensing may lead to certain limitations. For example, if the sensing and processing durations are too long, the Radiobot may miss certain changes in RF conditions in the currently non-sensed sub-bands. On the other hand, short sensing durations may lead to inaccurate sensing results.

Since our proposed detection/classification procedure applies to each of the sub-bands in the same way, in the following, we present the model formulation for a particular sub-band n. Hence, for brevity of notation, we drop the frequency sub-band index n in the following discussion.

A. Observed Signals Model

We denote by $N(t)$ the total number of signals at time t in the sub-band of interest. The corresponding IF signal $y(t)$ in Fig. 3 can be expressed as shown in (1) [25], where $x_l(t)$ denotes the l-th baseband signal that is to be modulated at a carrier frequency f_{c_l}. The l-th baseband equivalent linear time-variant (LTV) impulse response $h_l(\tau', t)$ denotes the response of the channel at the time t to an impulse that stimulated the channel between the l-th signal source and the Radiobot at time $t - \tau'$ [25], [26]. The receiver noise, denoted by $w(t)$, is assumed to be a white noise process with double-sided power spectral density (PSD) of $\frac{N_0}{2}$. The average noise power at the output of the sweeping IF filter will be $P_n = \frac{N_0 B}{2}$, where B is the IF filter bandwidth. The resulting signal-to-noise ratio (SNR) at the output of the IF filter will thus be $SNR = \frac{P_s}{P_n}$ where P_s is the received signal power.

B. Detection of RF Activities

In order to detect active RF signals, we propose to identify their carrier frequencies and the associated cyclic frequencies that are induced by the underlying periodicities of those signals. Note that, it is well-known that almost all man-made signals exhibit such underlying periodicities due to, for example, their symbol rates, coding schemes, packet/frame header structures and training symbol sequences, etc. [27]. In the following discussion, however, we will explicitly focus on the cyclic properties induced by the symbol and coding rates[1]. Using the discrete-frequency smoothing method [27] described below, we compute an estimate of the Spectral Correlation Function (SCF) $S_x^{\alpha}(t, f)$ for a general discrete signal $\{x(t - kT_s)\}_{k=0}^{M-1}$, for each sub-band, where T_s is the sampling period, and M is the number of samples. Note that, this implies that the total time duration over which the particular frequency sub-band was scanned is $T = MT_s$.

The FFT $\tilde{X}(t, f)$ of the sequence $\{x(t - kT_s)\}_{k=0}^{M-1}$ is defined in (2) over the set of frequencies $\{-\frac{f_s}{2}, -\frac{f_s}{2} + F_s, \cdots, \frac{f_s}{2} - F_s, \frac{f_s}{2}\}$, where $f_s = \frac{1}{T_s}$ is the sampling rate and $F_s = \frac{1}{MT_s}$ is the frequency increment and $a(t)$ is a triangular data tapering window [27].

$$\tilde{X}(t, f) = \sum_{k=0}^{M-1} a(t - kT_s)x(t - kT_s)e^{-j2\pi f(t-kT_s)}. \quad (2)$$

An estimate of the SCF can then be obtained as [27] based on the discrete-frequency smoothing method:

$$\tilde{S}_x^{\alpha}(t, f) = \frac{1}{LT}\sum_{\nu=-(L-1)/2}^{(L-1)/2} \tilde{X}(t, f + \frac{\alpha}{2} + \nu F_s)\tilde{X}^*(t, f - \frac{\alpha}{2} + \nu F_s),$$

[1]It is fairly straightforward to generalize the method to include other periodicities that might be present in any given signal.

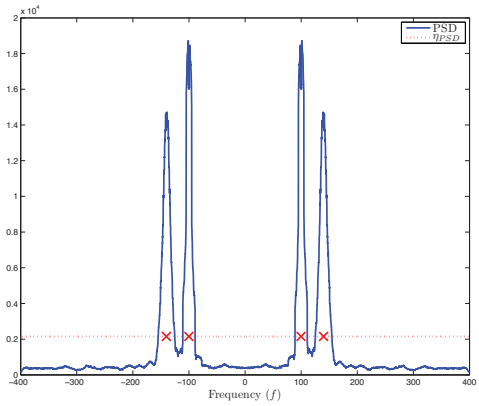

Fig. 4. Carrier frequencies are estimated as the midpoints of the intersections between the PSD curve and the threshold line.

where $T = MT_s$ is the time length of the data segment, α is the cyclic frequency and L (an odd number) is the spectral smoothing window length. By setting $\alpha = 0$, we first obtain an estimation of the power spectral density (PSD) of the discrete signal $\{x(t - kT_s)\}_{k=0}^{M-1}$:

$$\tilde{S}_x^0(t,f) = \frac{1}{LT} \sum_{\nu=-(L-1)/2}^{(L-1)/2} \left| \tilde{X}(t, f + \nu F_s) \right|^2 . \tag{3}$$

The active carrier frequencies in the spectrum sub-band of interest is determined by setting a threshold on the above PSD. According to [28], the threshold η_{PSD} shown below can be derived based on the Neyman-Pearson test:

$$\eta_{PSD} = \frac{\gamma^{-1}\left(L; (1-\alpha_F)\,\Gamma(L)\right) P_n}{T_s L} , \tag{4}$$

where α_F is the false alarm probability, γ^{-1} is the inverse lower incomplete gamma function (where $\gamma(k,x) = \int_0^x t^{k-1}e^{-t}dt$ and the inverse is w.r.t. the second argument), $\Gamma(k) = \int_0^\infty t^{k-1}e^{-t}dt$ is the gamma function and P_n is the noise power that can be estimated as $\hat{P}_n = T_s \sum_{f=-f_s/2}^{f_s/2} \tilde{S}_x^0(t,f)$, similar to [15], [29]. The impact of noise power uncertainty was discussed and analyzed in [30], [31] where the deterioration of the detector performance was upper-bounded by an expression involving the peak-to-peak range of noise uncertainty [30]. The carrier frequencies are estimated as the midpoints of the segments formed by the intersection between the PSD curve and the threshold line η_{PSD}, as shown in Fig. 4. We denote by $\mathcal{A}$ the set of all detected carrier frequencies in the sub-band of interest.

Next, an estimate of the spectral autocoherence function magnitude [27] is computed as:

$$|\tilde{C}_x^\alpha(t,f)| = \frac{|\tilde{S}_x^\alpha(t,f)|}{\sqrt{\tilde{S}_x^0(t, f+\alpha/2)\tilde{S}_x^0(t, f-\alpha/2)}} . \tag{5}$$

Note that $|\tilde{C}_x^\alpha(t,f)|$ is normalized to be between 0 and 1. Due to the fact that for each carrier, the associated cyclic components show up peaks in a close range of the carrier, we define the *cyclic sub-domain* profile of carrier $f_c \in \mathcal{A}$ as:

$$\tilde{I}_x(t,\alpha,f_c) = \max_{f \in [f_c - \Delta f_L(f_c), f_c + \Delta f_U(f_c)]} |\tilde{C}_x^\alpha(t,f)| , \tag{6}$$

where the lines $f = f_c - \Delta f_L(f_c)$ and $f = f_c + \Delta f_U(f_c)$ $(\forall f_c \in \mathcal{A})$ partition the (f,α)-plane into Voronoi cells whose point sites [32] are located at the detected carrier frequency points $\{(f_c, 0) : f_c \in \mathcal{A}\}$.

In [33], it is shown that digital signals exhibit cyclostationarity at multiples of their baud rates. Moreover, the digital signals may exhibit other periodicities as well, for example, due to coding. We denote the RF signature of the signal centered at f_c as $\mathrm{RF}(f_c) = \{\alpha \neq 0 : \mathfrak{I}_E \tilde{I}_x(t,\alpha,f_c) \geq \zeta\}$, where $\mathfrak{I}_E$ denotes the indicator function of event $E = \{\tilde{I}_x(t,\alpha,f_c)$ is a local maximum$\}$, and $\zeta \in (0,1)$ is a threshold for the peak detection in the cyclic sub-domain profile.

C. Spectral Correlation Function of Multiple Superposed Digital Signals

In practice, the Radiobot is more likely to deal with multiple RF activities in each spectrum sub-band of interest. Thus, it needs to know the corresponding SCF properties of superposed digital signals, in order to identify the number and types of the detected signals accurately.

In order to analyze the impact of the superposition of multiple signals on the SCF of a signal $y(t)$, let us assume that $y(t) = w(t) + \sum_{m=1}^{N_s} x_m(t)$, where $\{x_m(t)\}_{m=1}^{N_s}$ are independent zero-mean random processes (denoting N_s superposed signals) and $w(t)$ is an independent white noise process with a power spectral density of $\frac{N_0}{2}$. The autocorrelation function of $y(t)$ is $R_{yy}(t,\tau) = \frac{N_0}{2}\delta(\tau) + \sum_{m=1}^{N_s} R_{x_m x_m}(t,\tau)$, where $R_{x_m x_m}(t,\tau)$ is the autocorrelation functions of $x_m(t)$, for $m = 1, \cdots, N_s$. First, we define a Fourier Transform for the cyclic autocorrelation function as [34]:

$$\begin{aligned} R_{yy}^\alpha(\tau) &\triangleq \lim_{T\to\infty} \frac{1}{T} \int_{T/2}^{T/2} R_{yy}(t,\tau) e^{-j2\pi\alpha t} dt \\ &= \lim_{T\to\infty} \frac{1}{T} \int_{T/2}^{T/2} \left[\frac{N_0}{2}\delta(\tau) + \sum_{m=1}^{N_s} R_{x_m x_m}(t,\tau) \right] e^{-j2\pi\alpha t} dt \\ &= \frac{N_0}{2}\delta(\tau)\delta(\alpha) + \sum_{m=1}^{N_s} R_{x_m x_m}^\alpha(\tau) \end{aligned} \tag{7}$$

where $\delta(t)$ is the Dirac-delta function. The SCF can then be expressed as:

$$S_y^\alpha(f) = \int_{\mathbb{R}} R_{yy}^\alpha(\tau) e^{-j2\pi f\tau} d\tau = \frac{N_0}{2}\delta(\alpha) + \sum_{m=1}^{N_s} S_{x_m}^\alpha(f). \tag{8}$$

This result shows that the superposition of multiple independent signals results in a superposition of spectral peaks in the (f,α) domain. In other words, the SCF of the superposition of multiple signals has peaks at cyclic frequencies corresponding to integer multiples of, for example, the data rates of each signal.

D. Feature Extraction: Baud Rate and Coding Properties

The RF signature $\mathrm{RF}(f_c)$ vector itself can be used as a feature for classifying detected signals. For compactness, it is more convenient, however, to represent this vector by fewer elements. To achieve this, we define two feature elements α_1 and α_2 that are extracted from the RF signature, with α_1

representing the baud rate induced cyclic frequency and α_2 representing the coding induced cyclic frequency. Based on the cyclostationarity properties, the cyclic profile exhibits high peaks at the induced cyclic frequencies α_1 and α_2. Moreover, since the code length is usually a multiple of the symbol duration, the coding induced cyclic frequency α_2 is smaller than the data rate induced cyclic frequency α_1. By using this information, in Algorithm 1, a feature extraction procedure for determining α_1 and α_2 is proposed. Note that, in this algorithm, $\rho \in (0,1)$ with $\rho >> 0$.

Algorithm 1 Feature Extraction Procedure

for each $f_c \in \mathcal{A}$ **do**
  $F = [f_c - \Delta f_L, f_c + \Delta f_R]$
  $V_1 = \text{RF}(f_c)$, $M_1 = \arg\max_{\alpha \in V_1} \tilde{I}(t, \alpha, f_c)$
  $V_2 = \text{RF}(f_c) \backslash M_1$, $M_2 = \arg\max_{\alpha \in V_2} \tilde{I}(t, \alpha, f_c)$
  if $M_1 < M_2$ **then**
    if $\rho \tilde{I}(t, M_1, f_c) > \tilde{I}(t, M_2, f_c)$ **then**
      $(\alpha_1, \alpha_2) = (M_1, 0)$
    else
      $(\alpha_1, \alpha_2) = (M_2, M_1)$
    end if
  else
    $(\alpha_1, \alpha_2) = (M_1, M_2)$
  end if
end for

III. Impact of Channel Fading on the Cyclostationary Features

In this section, we show that the cyclostationary features of signals can essentially be preserved even in the presence of channel fading. In other words, we show that the proposed cyclostationarity based detection method is robust against channel fading effects.

A continuous-time real-valued stochastic process $x(t)$ is said to be second-order *cyclostationary in the wide sense* if its mean $\mathbb{E}\{x(t)\}$ and autocorrelation function $R_{xx}(t,\tau) \triangleq \mathbb{E}\{x(t+\tau)x(t)\}$ are periodic with some period, say T_0:

$$\mathbb{E}\{x(t+T_0)\} = \mathbb{E}\{x(t)\},\ R_{xx}(t+T_0,\tau) = R_{xx}(t,\tau), \quad (9)$$

for all t and τ [35]. We consider a cyclostationary digital signal $x(t)$ and an LTV fading channel (i.e. due to the Doppler effect), having an impulse response of $h(\tau', t)$. According to the definition of cyclostationarity, we know that the autocorrelation function of $x(t)$ is a periodic function of t, such that $R_{xx}(t+T_0,\tau) = R_{xx}(t,\tau)$, for some period T_0. The received signal $y(t)$ through the LTV fading channel can be expressed as:

$$y(t) = \int_0^\infty x(t-\tau')h(\tau', t)d\tau' + w(t), \quad (10)$$

where $w(t)$ is an additive wide sense stationary (WSS) noise process. The autocorrelation function of the received signal $y(t)$ can then be expressed as:

$$\begin{aligned}
&R_{yy}(t,\tau) = \mathbb{E}\{y(t+\tau)y(t)\} \\
&= \mathbb{E}\left\{\left[\int_0^\infty x(t+\tau-\tau_1')h(\tau_1', t+\tau)d\tau_1' + w(t+\tau)\right]\times\right. \\
&\left.\times\left[\int_0^\infty x(t+\tau-\tau_2')h(\tau_2', t)d\tau_2' + w(t)\right]\right\} \\
&= \mathbb{E}\left\{\int_0^\infty\int_0^\infty x(t+\tau-\tau_1')x(t+\tau-\tau_2')\times\right. \\
&\left.\times\ h(\tau_1', t+\tau)h(\tau_2', t)d\tau_1'd\tau_2'\right\} + \mathbb{E}\{w(t+\tau)w(t)\} \\
&= \int_0^\infty\int_0^\infty \mathbb{E}\{x(t+\tau-\tau_1')x(t+\tau-\tau_2')\}\times \\
&\times\ \mathbb{E}\{h(\tau_1', t+\tau)h(\tau_2', t)\}\, d\tau_1'd\tau_2' + R_{ww}(t,\tau) \\
&= \int_0^\infty\int_0^\infty R_{xx}(t,\tau-\tau_1'+\tau_2')\times \\
&\times\ R_{hh}(\tau_1', \tau_2'; t+\tau, t)d\tau_1'd\tau_2' + R_{ww}(\tau), \quad (11)
\end{aligned}$$

where $R_{hh}(\tau_1', \tau_2'; t_1, t_2) \triangleq \mathbb{E}\{h(\tau_1', t_1)h(\tau_2', t_2)\}$ is the autocorrelation of the channel impulse response $h(\tau', t)$, and $R_{ww}(t,\tau) = R_{ww}(\tau)$ is the autocorrelation function of the WSS noise.

According to empirical studies, the channel can be considered as WSS as long as the mobile unit covers a distance in the dimension of a few tens of the wavelength of the carrier signal in an observation period [36]. We also assume that scattering components with different propagation delays are statistically uncorrelated. These channel models are called US (uncorrelated scattering) channel models or US models [25]. The most important class of stochastic LTV channel models is represented by models belonging both to the class of WSS and to the class of US. These channel models are called WSSUS models which are almost exclusively employed in current literature for modeling frequency selective mobile radio channels [25], [36]–[39].

Under this common assumption of WSSUS, the autocorrelation function of the impulse response of the LTV fading channel can be expressed as [25]:

$$R_{hh}(\tau_1', \tau_2'; t+\tau, t) = \delta(\tau_2' - \tau_1')S_{hh}(\tau_1', \tau), \quad (12)$$

where $S_{hh}(\tau_1', \tau)$ is called the *delay cross-power spectral density* [25]. We substitute (12) back into (11) to obtain:

$$\begin{aligned}
R_{yy}(t,\tau) &= \int_0^\infty\int_0^\infty R_{xx}(t,\tau-\tau_1'+\tau_2')\times \\
&\times\ \delta(\tau_2'-\tau_1')S_{hh}(\tau_1',\tau)d\tau_1'd\tau_2' + R_{ww}(\tau) \\
&= \int_0^\infty R_{xx}(t,\tau)S_{hh}(\tau_1',\tau)d\tau_1' + R_{ww}(\tau) \\
&= R_{xx}(t,\tau)\int_0^\infty S_{hh}(\tau_1',\tau)d\tau_1' + R_{ww}(\tau) \quad (13)
\end{aligned}$$

so that

$$\begin{aligned}
R_{yy}(t+T_0,\tau) &= R_{xx}(t+T_0,\tau)\textstyle\int_0^\infty S_{hh}(\tau_1',\tau)d\tau_1' + R_{ww}(\tau) \\
&= R_{xx}(t,\tau)\textstyle\int_0^\infty S_{hh}(\tau_1',\tau)d\tau_1' + R_{ww}(\tau) \\
&= R_{yy}(t,\tau). \quad (14)
\end{aligned}$$

This shows that the autocorrelation function of the received signal $y(t)$ is also periodic with the same period T_0 as the

transmitted signal $x(t)$. As a result, the received signal $y(t)$ is also cyclostationary with the same cyclic components as $x(t)$.

A more general class of stochastic processes is obtained if the autocorrelation function $R_{xx}(t,\tau)$ is almost periodic in t for each τ [34]: A continuous-time real-valued stochastic process $x(t)$ is said to be *almost-cyclostationary (ACS) in the wide sense* if its autocorrelation function $R_{xx}(t,\tau)$ is an almost periodic function of t (with frequencies not depending on τ) [35]. When the input signal $x(t)$ is considered as ACS, the output signal $y(t)$ through the LTV fading channel is also ACS with the same cyclic components as $x(t)$, since we can see from (13) and (14) the autocorrelation function $R_{yy}(t,\tau)$ is also almost periodic with the same period as $R_{xx}(t,\tau)$.

As a result, we see that when fading channels are considered as general LTV systems, the cyclostationary properties of the transmitted signals are not altered at the output of the channel, or the received signal at the Radiobot. This justifies the robustness of the proposed cyclostationarity based detection/classification method in this paper, in the presence of channel fading. Note that, the proposed cyclostationarity based detection method introduced in Section II-B also applies to the ACS assumption, since the SCF is also defined under the assumption of ACS and it has been shown that an ACS signal exhibits cyclostationarity at cycle frequency α if $R^{\alpha}_{xx}(\tau) \not\equiv 0$, similarly to the cyclostationary stochastic processes [34], [35].

IV. Impact of the Doppler Shift on the Detected Carrier Frequencies

The cyclic autocorrelation function $R^{\alpha}_{yy}(\tau)$ of the received signal $y(t)$ is defined as $R^{\alpha}_{yy}(\tau) \triangleq \lim_{T\to\infty} \frac{1}{T}\int_{-\frac{T}{2}}^{\frac{T}{2}} R_{yy}(t,\tau)e^{-j2\pi\alpha t}dt$ [34]. Replacing $R_{yy}(t,\tau)$ by its value in (13), we obtain:

$$R^{\alpha}_{yy}(\tau) = H(\tau)R^{\alpha}_{xx}(\tau) + R_{ww}(\tau)\delta^{K}(\alpha), \tag{15}$$

where $H(\tau) = \int_{-\infty}^{\infty} S_{hh}(\tau_1',\tau)d\tau_1'$ and δ^K denotes the Kronecker delta function. We may compute the PSD $S^0_y(f)$ of the received signal $y(t)$ as the Fourier transform (denoted by the operator $\mathcal{F}$) of $R^{\alpha}_y(\tau)$ at $\alpha = 0$, such that:

$$\begin{aligned} S^0_y(f) &= \mathcal{F}\left\{\int_{-\infty}^{\infty} S_{hh}(\tau_1',\tau)d\tau_1'\right\} * S^0_x(f) + S_w(f) \\ &= \int_{-\infty}^{\infty} \mathcal{F}\left\{S_{hh}(\tau_1',\tau)\right\} d\tau_1' * S^0_x(f) + S_w(f) \\ &= \int_{-\infty}^{\infty} S(\tau_1',f)d\tau_1' * S^0_x(f) + S_w(f) \qquad (16) \\ &= S_{\mu\mu}(f) * S^0_x(f) + S_w(f)\ , \qquad (17) \end{aligned}$$

where $S(\tau_1',f)$ and $S_{\mu\mu}(f)$ are, respectively, the *scattering function* and the *Doppler power spectral density*, and $S^0_x(f)$ is the PSD of the transmitted signal. Note that (16) and (17) are obtained using (7.37) and (7.42) in [25], respectively.

The Doppler PSD is usually defined over a range $[-f_{max}, f_{max}]$, where f_{max} is the maximum Doppler frequency shift [25]. Thus, the received PSD can be expressed as:

$$S^0_y(f) = \int_{-f_{max}}^{f_{max}} S_{\mu\mu}(\nu)S^0_x(f-\nu)d\nu + S_{ww}(f)\ . \tag{18}$$

Based on (18), the convolution of $S^0_x(f)$ with a window of length $2f_{max}$ causes the PSD to spread at most by $\pm f_{max}$ at each point. If the Doppler PSD $S_{\mu\mu}(f)$ is symmetric (such as Jakes' type [25]), the carrier frequency components of the detected feature points do not shift since the main lobes of the PSD are spread evenly in both left and right directions. However, if $S_{\mu\mu}(f)$ is not symmetric (such as Rice's, Gauss I or Gauss II types [25]), the detected carrier frequencies will shift by an amount smaller than f_{max}. Therefore, due to the Doppler shift, it may not be possible to detect and distinguish signals that are separated by less than f_{max} in the spectrum. However, based on the users activity and by using appropriate learning algorithms, the Radiobot might be able to detect each of the signals when they are the only transmitted signals. Then using this knowledge, it may be able to distinguish them when both signals are transmitted simultaneously. This again emphasizes the importance of true learning from past experience during the signal detection and classification steps.

V. Autonomous Signal Classification using the CRP

In the following, we develop a non-parametric technique to obtain statistical information on the association of cyclic frequencies and carrier frequencies. Many existing unsupervised machine learning techniques used for classifications rely on certain assumptions on the data, such as the number of classes present. However, a non-parametric approach makes few assumptions about the distribution from which the data is drawn [14], [40], [41]. We believe this is the appropriate framework so as to enable the Radiobot to work in a wide-range of possible RF environments which may contain arbitrary number of wireless systems with arbitrary number of users in each system at any given time. The non-parametric model used in this paper is based on the Dirichlet Process Mixture Model (DPMM) [14], [41], [42], in which, the number of clusters/mixtures present in data is not known *a priori*. In contrast with parametric approaches, such as the Gaussian mixture model (GMM) and K-means classification methods, non-parametric classification methods assume an unknown number of mixture components while assigning each observed feature point to a corresponding cluster. Hence, non-parametric classification methods can infer the number of clusters from the data itself, making them suitable for identifying the number of RF systems in an unknown environment. Thus, we propose the DPMM as a framework for classifying the observed feature points in the RF environment. A description of the DPMM can be found, for example, in [14], [41].

Let us define a q-dimensional (where q could also be infinite) feature vector $\boldsymbol{\theta}$. The elements of each feature vector $\boldsymbol{\theta}$ include the observed carrier frequency and the different cyclic components, which determine the RF signature of a sensed signal. The q-dimensional feature vector is denoted by $\boldsymbol{\theta} = (f_c, \alpha_1, \cdots, \alpha_{q-1})^T$, where $\alpha_i \in \mathbb{R}$ represents the i-th cyclic component in the signal centered at f_c. In practice, of course, it is not possible to observe the feature $\boldsymbol{\theta}$ directly, instead we get a noisy observation vector $\mathbf{z} = (z_1, \cdots, z_q)^T$. Generally, this noise depends on the environment, numerical approximations, quantization errors in ADC's and estimation errors. Thus, the observed feature vector can be modeled as:

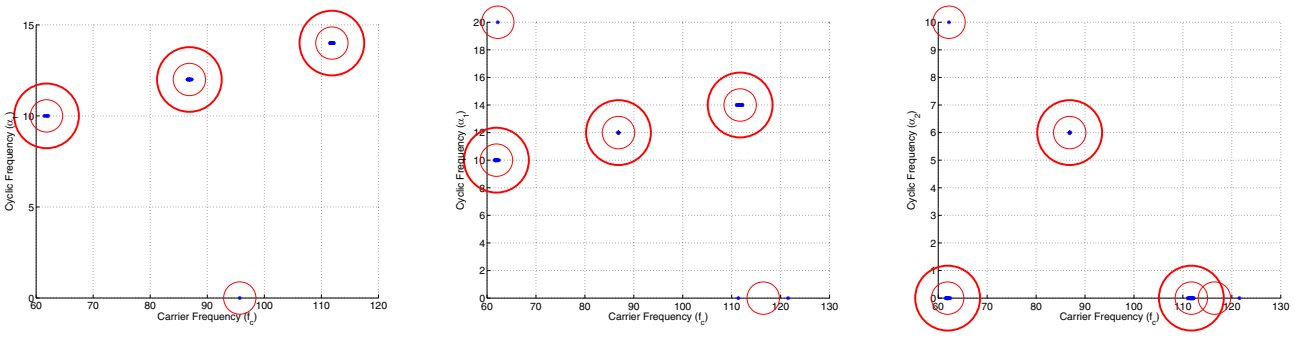

(a) (f_c, α_1)-plane (Without Coding). (b) (f_c, α_1)-plane (With Coding on channel 2). (c) (f_c, α_2)-plane (With Coding on channel 2).

Fig. 5. CRP-based data clustering with active carrier frequencies $f_c = 62, 87, 112$ MHz, symbol rates 10, 12 and 14 Mbaud, respectively.

$\mathbf{z} = \boldsymbol{\theta} + \mathbf{v}$, where $\mathbf{v}$ is assumed as a Gaussian noise vector of *independent* components, capturing the environmental noise and estimation errors, as in [15][2]. Each observation $\mathbf{z}$ is classified into clusters $\{\mathcal{C}_i : i = 1, 2, \cdots\}$, with each cluster representing a certain RF system or a class of signals having similar RF characteristics. We denote the cluster centers by $\{\boldsymbol{\mu}_i : i = 1, 2, \cdots\}$ and corresponding covariance matrices by $\{\boldsymbol{\Sigma}_i : i = 1, 2, \cdots\}$. Each cluster center $\boldsymbol{\mu}_i$ is an unbiased estimate of its associated feature vector $\boldsymbol{\theta}_i$. We denote the cluster assignment variable by $\Lambda \in \{1, 2, \cdots\}$ which represents a certain class of systems that share a common RF characteristic. In general, the properties of a cluster $\Lambda \in \{1, 2, \cdots\}$ (for example, its mean and covariance) are unknown and to be estimated from the observed feature points themselves. For each observation $\mathbf{z}$, we apply the Maximum a Posteriori (MAP) rule to assign $\mathbf{z}$ into the cluster $\hat{\lambda}(\mathbf{z})$, such that: $\hat{\lambda}(\mathbf{z}) = \arg\max_{i \in \{1, \cdots\}} \Pr\{\mathbf{z}|\Lambda = i\}\Pr\{\Lambda = i\}$. The likelihood of $\mathbf{z}$ being in cluster $\mathcal{C}_i$ is $\Pr\{\mathbf{z}|\Lambda = i\} = \prod_{k=1}^{q} f(z_k|\mu_{i,k}, \sigma_{i,k})$, where $f(z|\mu, \sigma)$ is the probability density function (pdf) of a Gaussian random variable $Z \sim \mathcal{N}(\mu, \sigma^2)$. After each assignment, we update the center and covariance matrix of the corresponding cluster. Given a sequence of cluster assignments $\Lambda_1, \cdots, \Lambda_m$, by using the DPMM properties, the probability distribution of Λ_{m+1} is:

$$\Lambda_{m+1}|\Lambda_1, \cdots, \Lambda_m \sim \frac{1}{\alpha_D + m}\left(\alpha_D H + \sum_{k=1}^{p} n_k \delta_{\Lambda_k^*}\right), \quad (19)$$

where $\Lambda_1^*, \cdots, \Lambda_p^*$ are the unique values among $\Lambda_1, \cdots, \Lambda_m$ (corresponding to p distinct clusters), n_k is the number of repeats of Λ_k^* (i.e. number of feature points in cluster Λ_k^*), δ_Λ is a point mass located at Λ, and $\sim$ is shorthand for "is distributed as". The probability distribution H represents a prior distribution of the cluster assignment variables, based on previous knowledge. If no such knowledge is available, the choice of H can be made irrelevant by setting $\alpha_D = 0$. Note that, if $\max_{i \in \{1, \cdots\}} \Pr\{\Lambda = i|\mathbf{z}\} \leq \delta$ (for some $\delta > 0$), we create a new cluster $\mathcal{C}$ centered at $\mathbf{z}$ and with a suitably chosen covariance matrix.

[2]While Gaussianity is assumed here for simplicity to illustrate our concepts, better noise models are to be investigated in our on-going work.

VI. Self-Reconfiguration of the Spectrum Sensing Module

The performance of the Radiobot is related to the quality and accuracy of the sensing observations. It is required to optimize the sensing module so that it best estimates the RF activity in the surrounding environment. Several parameters may need to be optimized during the sensing process, such as the sensing duration, detector thresholds, spectrum sensing policies, etc. based on the particular RF environment it encounters at a given time. It is the task of the learning and reasoning abilities of the Radiobot to make the CE dynamically adapt these parameters based on its past experience. To be specific, assume that the Radiobot needs to optimize its cyclic sub-profile threshold ζ such that it achieves a certain false alarm probability. Of course, it is almost impossible to obtain analytical solutions to this problem due to the complexity of the cyclic profile equation and to the uncertainty in the surrounding environment. A possible solution is to learn the optimal threshold value iteratively based on the sensing observations, as in [19].

An online learning algorithm was proposed in [19] to adapt the threshold value of Neyman-Pearson test when the probability distribution of the detected signals is unknown. The threshold is thus dynamically updated to achieve a desired false-alarm probability. The learning process is conducted during a training period in which the observed data are drawn from a null hypothesis. In our case, however, we do not assume a training period and we propose a learning algorithm that updates the cyclic sub-profile threshold ζ during the normal operation time itself to achieve a desired false alarm probability ϕ. By the help of the energy detection, the learning algorithm identifies the absence of transmitted signals to perform the learning process. The objective of the learning algorithm is to minimize the Kullback-Leibler distance $K(P||Q)$ between two probability distributions P and Q, similar to [19], where:

$$K(P||Q) = \sum_i P(i) \log \frac{P(i)}{Q(i)}. \quad (20)$$

We denote by P and Q the desired and actual probability distributions of the cyclostationary detector output, conditioned on the absence of transmitted signals. These probability distributions correspond to Bernoulli random variables, representing

whether a signal is (1) or is not (0) detected. By defining ϕ and $P_f(\zeta)$ as the desired and actual false alarm probabilities (for a given threshold ζ), respectively, the Kullback-Leibler distance can then be expressed as:

$$K(P||Q) = K(\phi, P_f(\zeta)) = \phi \log \frac{\phi}{P_f(\zeta)} + (1-\phi) \log \frac{1-\phi}{1-P_f(\zeta)} . \quad (21)$$

Note that $K(\phi, P_f(\zeta)) = 0$ iff $\phi = P_f(\zeta)$. Due to its convexity in $P_f(\zeta)$, the Kullback-Leibler distance guarantees a global minimum. Moreover, it was shown in [19] that $K(\phi, P_f(\zeta))$ is convex in ζ iff $P_f(\zeta)$ is monotonous, which is satisfied in our case. However, since the analytical expression of $P_f(\zeta)$ is unknown, it can be estimated as the ratio of sample points that exceed the threshold ζ in the cyclic profile $I(\alpha)$, when there is no transmitted signals. As noted in [19], to achieve accurate estimate for $P_f(\zeta)$, the recursive adaptation in ζ should not be too frequent. This is taken into account in the proposed learning algorithm (Algorithm 2), in which the threshold ζ is updated after each $N_c > 1$ updates of the false alarm probability $P_f(\zeta)$.

Algorithm 2 Learning algorithm to control the cyclic sub-profile threshold ζ

Initialize: $counter = 1$.
while No signal is detected by the energy detector **do**
  Update the false alarm probability $P_f(\zeta)$ and $counter = counter + 1$.
  if $counter = N_c$ **then**
    Update ζ such that: $\zeta \leftarrow \zeta + \psi\,(P_f(\zeta) - \phi)$.
    Reset $counter = 1$.
  end if
end while

The update rule in Algorithm 2 minimizes the Kullback-Leibler function since it follows a gradient descent direction that reduces the difference $|P_f(\zeta) - \phi|$ at a learning rate of $\psi > 0$. Moreover, due to the convexity of the Kullback-Leibler function, this algorithm is guaranteed to converge to a unique optimal threshold value.

VII. Simulation Results

In order to demonstrate the performance of our proposed cyclostationarity-based autonomous signal detection and classification procedure, we simulate several signals in the $2.4GHz$ ISM band. These signals are assumed to have carriers at $2.412GHz$, $2.437GHz$ and $2.462GHz$ and symbol rates of 10, 12 and 14 Mbauds, respectively. The signals are allowed to use different QAM schemes and are equally likely to be in ON or OFF states during each sensing period. Wireless channel is assumed to be Rayleigh fading. The fading channels coefficients h are normalized, such that $\mathbb{E}\{h^2\} = 1$. Also, the Radiobot's receiver is subjected to white Gaussian noise.

We assume that the sensed signal is downconverted to IF band with an IF oscillator with frequency of $f_I = 2.35GHz$. After IF conversion, the three signals are supposed to be centered at 62, 87 and 112 MHz. Each sensing observation takes $12\mu s$ with a receiver SNR of $20dB$.

Initially, we assume that the signals are not coded and we plot the detected feature points $(f_c, \alpha_1, \alpha_2)$ in Fig. 5(a), where

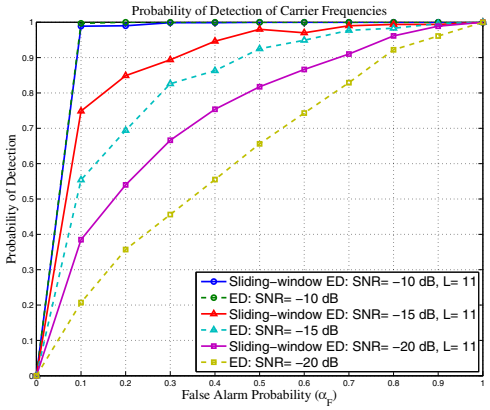

Fig. 6. Comparison between the receiver operating characteristics (ROC's) of the sliding-window and conventional energy detections. The sliding-window length is $L = 11$.

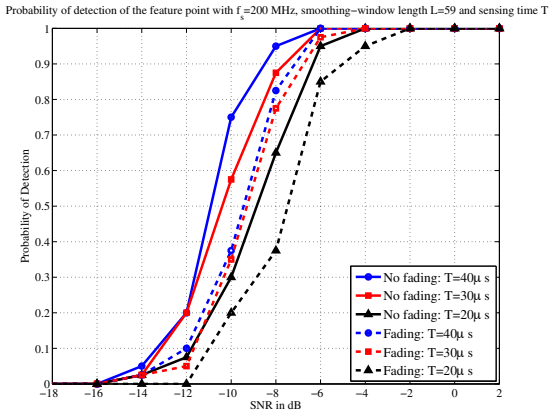

Fig. 7. Probability of identification of feature points with a sampling frequency $f_s = 200MHz$ and sliding-window length $L = 59$. The detected signal is a 4-QAM with symbol rate of 5 Mbauds and down-converted to a carrier frequency of $20MHz$. The performance is compared under both non-fading and Rayleigh fading channels.

it is found that $\alpha_2 = 0$ (meaning that no coding is detected). We observe that the carrier frequencies and symbol rates were accurately specified for each system. Also, we use bold circles to represent the clusters that occur with a probability higher than 0.1. We remark that an erroneous feature point is detected at $\alpha_1 = 0$. However, its corresponding cluster has a very low probability, thus it can be neglected in the sensing outcome.

Next, we repeat the same simulation, but assuming that the system on channel 2 uses a coding with rate $1/2$. The coding rate is manifested through the feature α_2 which is expected to be equal to $1/2$ times the symbol rate of the second signal. We plot the result in Fig. 5(b) and Fig. 5(c). As expected, the signals on the first and third channels that are not using a coding structure have $\alpha_2 = 0$. Only the signal on channel 2 has an $\alpha_2 = 6$, which corresponds to its coding rate.

In Fig. 6, we show the ROC curves of the adopted sliding-window energy detection scheme [28], [43]. This detector is compared to the conventional energy detection and it shows superior detection performance. Next, we show in Fig. 7 the detection performance of the cyclostationary detection for different values of SNR's and for different sensing times.

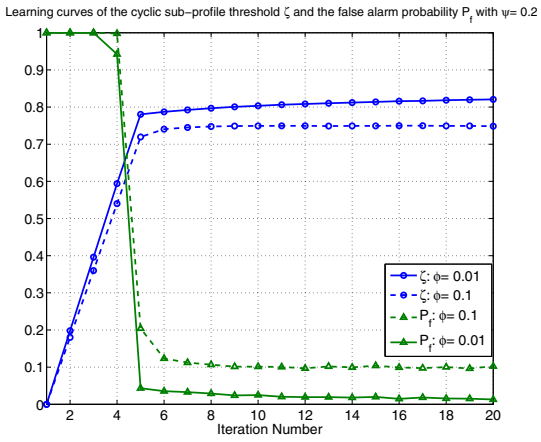

Fig. 8. Learning curves of the cyclic sub-profile threshold ζ and the false alarm probability P_f with a learning rate $\psi = 0.2$ and a desired false alarm probability ϕ (with $L = 11$).

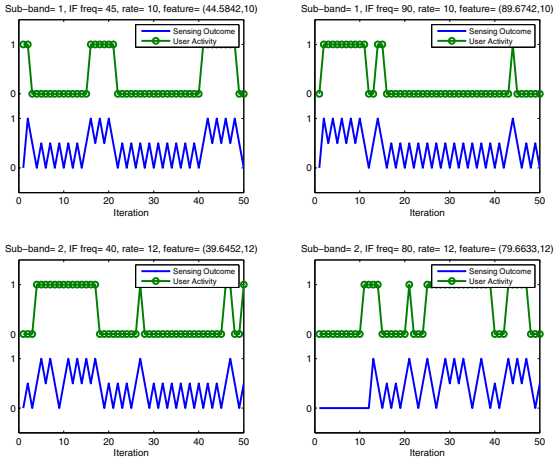

Fig. 9. Detection of multiple users in 2 separate sub-bands.

The results show that 95% of detection probability can be achieved at an SNR of $-6dB$ and with a sensing time of $T = 30\mu s$. Afterwards, we verify, in Fig. 8, the convergence of the learning algorithm proposed in Section VI. We let ϕ to be the desired false alarm probability of the cyclostationary detection and let ζ be the control threshold. Starting from $\zeta = 0$, Algorithm 2 converges to constant threshold at which the actual false alarm probability $P_f(\zeta)$ converges to ϕ. The learning rate is set to $\psi = 0.2$ and the threshold ζ is updated after each $N_c = 20$ updates of the false alarm probability $P_f(\zeta)$. Note that a similar learning procedure could be applied to adapt the energy detector threshold η_{PSD}. However, this step is not required in our case since we have an analytical expression for η_{PSD} in (4).

Finally, in order to verify the multi-band operability of the Radiobot, we simulate, in Fig. 9, the sequential sensing in two different sub-bands. Each sub-band has 2 different systems and we assume that these users can be either ON (1) or OFF (0) at each time instant, as shown in the user activity curves of Fig. 9. The Radiobot senses sequentially these sub-bands. We plot the sensing outcomes and represent by 1 (resp. 0) whether the corresponding system is detected (resp. not detected). An outcome of 0.5 implies that the corresponding sub-band is not sensed at a certain time. The results in Fig. 9 show that the Radiobot can accurately detect the different systems and allocate them to appropriate clusters, while switching between different sub-bands.

VIII. Conclusion

In this paper, we have proposed an autonomous CR architecture, referred to as the Radiobot [5]. This model is aimed at emphasizing the cognitive aspects of CR's by requiring that the Radiobot is able to achieve self-learning and self-reconfigurability. In this paper, a Radiobot employs a joint energy/cyclostationary detection to extract different features from the sensed signals. It then applies a DPMM-based clustering method to identify/classify the observed signals. A learning algorithm is proposed to allow self-reconfigurability of the Radiobot sensing module to match its RF environment. We analyzed the performance of the energy detection through the ROC and showed the robustness of the cyclostationary detection to fading and to wide-sense stationary noise. We verified, through simulations, the expected convergence of the proposed learning algorithm and the multi-band operability of the Radiobot architecture with the proposed wideband spectrum sensing approach..

References

[1] J. Mitola, III and G. Maguire, Jr., "Cognitive radio: making software radios more personal," *IEEE Personal Commun.*, vol. 6, no. 4, pp. 13–18, Aug. 1999.

[2] S. Haykin, "Cognitive radio: brain-empowered wireless communications," *IEEE J. Sel. Areas Commun.*, vol. 23, no. 2, pp. 201–220, Feb. 2005.

[3] N. Devroye, M. Vu, and V. Tarokh, "Cognitive radio networks," *IEEE Signal Process. Mag.*, vol. 25, no. 6, pp. 12–23, Nov. 2008.

[4] A. Goldsmith, S. Jafar, I. Maric, and S. Srinivasa, "Breaking spectrum gridlock with cognitive radios: an information theoretic perspective," *Proc. IEEE*, vol. 97, no. 5, pp. 894–914, May 2009.

[5] S. K. Jayaweera and C. G. Christodoulou, "Radiobots: architecture, algorithms and realtime reconfigurable antenna designs for autonomous, self-learning future cognitive radios," University of New Mexico, Technical Report EECE-TR-11-0001, Mar. 2011. Available: http://repository.unm.edu/handle/1928/12306

[6] J. Mitola, "Cognitive radio architecture evolution," *Proc. IEEE*, vol. 97, no. 4, pp. 626–641, Apr. 2009.

[7] Y. Tachwali, F. Basma, and H. Refai, "Cognitive radio architecture for rapidly deployable heterogeneous wireless networks," *IEEE Trans. Consum. Electron.*, vol. 56, no. 3, pp. 1426–1432, Aug. 2010.

[8] K. Smitha and A. Vinod, "A reconfigurable low complexity architecture for channel adaptation in cognitive radio," in *Proc. 2008 IEEE International Symposium on Personal, Indoor and Mobile Radio Communications*, pp. 1–5.

[9] S. Wang, H. Zhao, B. Zhang, H. Liu, and L. Xie, "An autonomic communication based conceptual and architecture model for cognitive radio nodes," in *Proc. 2010 IET International Conference on Wireless, Mobile and Multimedia Networks*, pp. 200–204.

[10] S. Maleki, A. Pandharipande, and G. Leus, "Two-stage spectrum sensing for cognitive radios," in *Proc. 2010 IEEE International Conference on Acoustics Speech and Signal Processing*, pp. 2946–2949.

[11] L. Luo, N. Neihart, S. Roy, and D. Allstot, "A two-stage sensing technique for dynamic spectrum access," *IEEE Trans. Wireless Commun.*, vol. 8, no. 6, pp. 3028–3037, June 2009.

[12] M. Ramon, T. Atwood, S. Barbin, and C. Christodoulou, "Signal classification with an SVM-FFT approach for feature extraction in cognitive radio," in *Proc. 2009 SBMO/IEEE MTT-S International Microwave and Optoelectronics Conference*, pp. 286–289.

[13] H. Hu, J. Song, and Y. Wang, "Signal classification based on spectral correlation analysis and SVM in cognitive radio," in *Proc. 2008 International Conference on Advanced Information Networking and Applications*, pp. 883–887.

[14] Y. W. Teh, "Dirichlet processes," in *Encyclopedia of Machine Learning*. Springer, 2007.
[15] N. Shetty, S. Pollin, and P. Pawelczak, "Identifying spectrum usage by unknown systems using experiments in machine learning," in *Proc. 2009 IEEE Wireless Communications and Networking Conference*, pp. 1–6.
[16] A. Galindo-Serrano and L. Giupponi, "Distributed Q—learning for aggregated interference control in cognitive radio networks," *IEEE Trans. Veh. Technol.*, vol. 59, no. 4, pp. 1823–1834, May 2010.
[17] J. Lunden, V. Koivunen, S. Kulkarni, and H. Poor, "Reinforcement learning based distributed multiagent sensing policy for cognitive radio networks," in *Proc. 2011 IEEE Symposium on New Frontiers in Dynamic Spectrum Access Networks*, pp. 642–646.
[18] M. Bkassiny, S. K. Jayaweera, and K. A. Avery, "Distributed reinforcement learning based MAC protocols for autonomous cognitive secondary users," in *Proc. 2011 Wireless and Optical Communications Conference*, pp. 1–6.
[19] D. Pados, P. Papantoni-Kazakos, D. Kazakos, and A. Koyiantis, "On-line threshold learning for Neyman-Pearson distributed detection," *IEEE Trans. Syst., Man Cybernetics*, vol. 24, no. 10, pp. 1519–1531, Oct. 1994.
[20] T. Atwood, "RF channel characterization for cognitive radio using support vector machines," Ph.D. dissertation, University of New Mexico, Nov. 2009.
[21] C.-C. Huang, C.-Y. Wang, and J.-T. Wu, "A CMOS 6-bit 16-gs/s time-interleaved ADC using digital background calibration techniques," *IEEE J. Solid-State Circuits*, vol. 46, no. 4, pp. 848–858, Apr. 2011.
[22] 12-Bit, 1-GSPSAnalog-to-Digital Converter. Available: http://focus.ti.com/lit/ds/symlink/ads5400.pdf
[23] D. Wieruch and V. Pohl, "A cognitive radio architecture based on sub-Nyquist sampling," in *Proc. 2011 IEEE Symposium on New Frontiers in Dynamic Spectrum Access Networks*, pp. 576–585.
[24] Y. Tawk, J. Costantine, K. Avery, and C. Christodoulou, "Implementation of a cognitive radio front-end using rotatable controlled reconfigurable antennas," *IEEE Trans. Antennas Propag.*, vol. 59, no. 5, pp. 1773–1778, May 2011.
[25] M. Patzold, *Mobile Fading Channels*, 1st edition. John Wiley & Sons, Ltd., 2002.
[26] A. Goldsmith, *Wireless Communications*, 1st edition. Cambridge University Press, 2005.
[27] W. Gardner, "Measurement of spectral correlation," *IEEE Trans. Acoustics, Speech Signal Process.*, vol. 34, no. 5, pp. 1111–1123, Oct. 1986.
[28] M. Bkassiny, S. K. Jayaweera, Y. Li, and K. A. Avery, "Blind cyclostationary feature detection based spectrum sensing for autonomous self-learning cognitive radios," in *2012 IEEE International Conference on Communications*.
[29] F. Millioz and N. Martin, "Estimation of a white Gaussian noise in the short time Fourier transform based on the spectral kurtosis of the minimal statistics: application to underwater noise," in *Proc. 2010 IEEE International Conference on Acoustics Speech and Signal Processing*, pp. 5638–5641.
[30] A. Sonnenschein and P. Fishman, "Radiometric detection of spread-spectrum signals in noise of uncertain power," *IEEE Trans. Aerospace and Electron. Syst.*, vol. 28, no. 3, pp. 654–660, July 1992.
[31] B. Shent, L. Huang, C. Zhao, Z. Zhou, and K. Kwak, "Energy detection based spectrum sensing for cognitive radios in noise of uncertain power," in *Proc. 2008 International Symposium on Communications and Information Technologies*, pp. 628–633.
[32] O. Setter, M. Sharir, and D. Halperin, "Constructing two-dimensional Voronoi diagrams via divide-and-conquer of envelopes in space," in *Proc. 2009 International Symposium on Voronoi Diagrams*, pp. 43–52.
[33] W. Gardner, W. Brown, and C.-K. Chen, "Spectral correlation of modulated signals—part II: digital modulation," *IEEE Trans. Commun.*, vol. 35, no. 6, pp. 595–601, June 1987.
[34] W. Gardner, A. Napolitano, and L. Paura, "Cyclostationarity: half a century of research," *Signal Process.*, vol. 86, no. 4, pp. 639–697, Apr. 2006. Available: http://dx.doi.org/10.1016/j.sigpro.2005.06.016
[35] W. A. Gardner, *Introduction to Random Processes: With Applications to Signals and Systems*, 2nd edition. McGraw-Hill, 1990.
[36] J. Parsons and A. Bajwa, "Wideband characterisation of fading mobile radio channels," *Commun., Radar and Signal Process., IEE Proceedings F*, vol. 129, no. 2, p. 95, Apr. 1982.
[37] D.-S. Yoo and W. Stark, "Characterization of wssus channels: normalized mean square covariance," *IEEE Trans. Wireless Commun.*, vol. 4, no. 4, pp. 1575–1584, July 2005.
[38] P. Hoeher, "A statistical discrete-time model for the WSSUS multipath channel," *IEEE Trans. Veh. Technol.*, vol. 41, no. 4, pp. 461–468, Nov. 1992.
[39] K.-W. Yip and T.-S. Ng, "Discrete-time model for digital communications over a frequency-selective Rician fading wssus channel," *IEE Proc.-Commun.*, vol. 143, no. 1, pp. 37–42, Feb. 1996.
[40] E. Fox, E. Sudderth, M. Jordan, and A. Willsky, "Bayesian nonparametric methods for learning Markov switching processes," *IEEE Signal Process. Mag.*, vol. 27, no. 6, pp. 43–54, Nov. 2010.
[41] Y. W. Teh, M. I. Jordan, M. J. Beal, and D. M. Blei, "Hierarchical Dirichlet processes," *J. Amer. Statistical Assoc.*, vol. 101, no. 476, pp. 1566–1581, Dec. 2006.
[42] T. S. Ferguson, "A Bayesian analysis of some nonparametric problems," *The Annals of Statistics*, vol. 1, no. 2, pp. 209–230, 1973. Available: http://dx.doi.org/10.2307/2958008
[43] Y. M. Kim, G. Zheng, S. H. Sohn, and J. M. Kim, "An alternative energy detection using sliding window for cognitive radio system," in *Proc. 2008 International Conference on Advanced Communication Technology*, vol. 1, pp. 481–485.

Mario Bkassiny (S'06) received the B.E. degree in Electrical Engineering and the M.S. degree in Computer Engineering both from the Lebanese American University, Lebanon, in 2008 and 2009, respectively. He is currently working towards the PhD degree in Electrical Engineering at the Communication and Information Sciences Laboratory (CISL), Department of Electrical and Computer Engineering at the University of New Mexico, Albuquerque, NM, USA. His current research interests are in cognitive radios, distributed learning and reasoning, cooperative communications, dynamic spectrum leasing and game theory.

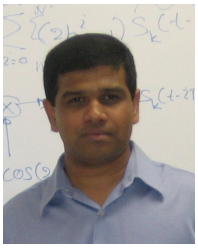

Sudharman K. Jayaweera (S'00, M'04, SM'09) received the B.E. degree in Electrical and Electronic Engineering with First Class Honors from the University of Melbourne, Australia, in 1997 and M.A. and PhD degrees in Electrical Engineering from Princeton University in 2001 and 2003, respectively. He is currently an assistant Professor in Electrical Engineering at the Department of Electrical and Computer Engineering at University of New Mexico, Albuquerque, NM. From 2003-2006 he was an assistant Professor in Electrical Engineering at the Department of Electrical and Computer Engineering at Wichita State University. Dr. Jayaweera is currently an associate editor of *EURASIP Journal on Advances in Signal Processing*. His current research interests include cooperative and cognitive communications, information theory of networked-control systems, statistical signal processing and wireless sensor networks.

Yang Li received the B.E. degree in Electrical Engineering from the Beijing University of Aeronautics and Astronautics, Beijing, China, in 2005 and the M.S. degree in Electrical Engineering from New Mexico Institute of Mining and Technology, Socorro, New Mexico, USA in 2009. He is currently working towards the PhD degree in Electrical Engineering at the Communication and Information Sciences Laboratory (CISL), Department of Electrical and Computer Engineering at the University of New Mexico, Albuquerque, NM, USA. His current research interests are in cognitive radios, spectrum sensing, cooperative communications, and dynamic spectrum access.

Keith A. Avery is the Program Lead for the Integrated Microsystems program at the Air Force Research Laboratory focusing on advanced packaging and optoelectronics for space. He received his BS degree from DeVry Institute of Technology in 1983. For the first 12 years of his career he worked in the commercial sector designing digital and analog circuits for commercial, industrial, and telephony applications. Prior to joining AFRL he worked as a government contractor performing design activities for space experiments, advanced packaging techniques, and radiation effects on micro-electronics. During his career he has increased his level of responsibility for design activities and program management. He has authored or co-authored numerous papers on designs for space and radiation effects. Mr. Avery is a member of IEEE/NPSS and AIAA.